Precision measurement of scaled momentum, charge multiplicity and thrust in $\nu\_\mu N$ and $\overline{\nu}\_\mu N$ Interactions

J. Altegoer, C. Angelini, P. Astier, D. Autiero, A. Baldisseri, M. Baldo-Ceolin, G. Ballocchi, M. Banner, S. Basa, G. Bassompierre, et al.

EUROPEAN ORGANIZATION FOR NUCLEAR RESEARCH

CERN-EP/98-179
19th November 1998

Precision Measurement of Scaled Momentum, Charge Multiplicity and Thrust in ν_μ N and $\bar{\nu}_\mu$ N Interactions

The NOMAD Collaboration

Abstract

We report the first precision measurements of the scaled momentum, the charge multiplicity, and the thrust of hadronic jets in the Breit frame in Deep Inelastic Scattering ν_μ N and $\bar{\nu}_\mu$ N charged current events over the Q^2 range from 1 to 100 GeV^2 . The neutrino data, obtained in the NOMAD experiment at the CERN SPS, extend the Q^2-evolution of these parameters by two orders of magnitude, and with commensurate precision, when compared to those reported by the ep and e^+e^- experiments.

(to be published in Physics Letters B)

J. Altegoer[5] C. Angelini[16] P. Astier[14] D. Autiero[8] A. Baldisseri[18] M. Baldo-Ceolin[13] G. Ballocchi[8] M. Banner[14] S. Basa[9] G. Bassompierre[1] K. Benslama[9] N. Besson[18] I. Bird[9,8] B. Blumenfeld[2] F. Bobisut[13] J. Bouchez[18] S. Boyd[19] A. Bueno[3] S. Bunyatov[6] L. Camilleri[8] A. Cardini[10] P.W. Cattaneo[15] V. Cavasinni[16] A. Cervera-Villanueva[8] G. Collazuol[13] G. Conforto[21,8] C. Conta[15] M. Contalbrigo[13] R. Cousins[10] D. Daniels[3] H. Degaudenzi[9] A. De Santo[16,8] T. Del Prete[16] T. Dignan[3] L. Di Lella[8] E. do Couto e Silva[8] I.J. Donnelly[19,20] J. Dumarchez[14] M. Ellis[19] T. Fazio[1] G.J. Feldman[3] R. Ferrari[15] D. Ferrère[8] V. Flaminio[16] M. Fraternali[15] J-M. Gaillard[1] P. Galumian[9] E. Gangler[14] A. Geiser[8,5] D. Geppert[5] D. Gibin[13] S. Gninenko[12] A. Godley[19] J-J. Gomez-Cadenas[22,8] J. Gosset[18] C. Gößling[5] M. Gouanère[1] A. Grant[8] G. Graziani[7] A. Guglielmi[13] C. Hagner[18] J. Hernando[22,26] D. Hubbard[3] P. Hurst[3] N. Hyett[11] E. Iacopini[7] C. Joseph[9] F. Juget[9] M. Kirsanov[12] O. Klimov[6] J. Kokkonen[8] A. Kovzelev[12] A. Krasnoperov[1,6] V.E. Kuznetsov[6,8] S. Lacaprara[13] A. Lanza[15] L. La Rotonda[4] M. Laveder[13] C. Lazzeroni[16] A. Letessier-Selvon[14] J-M. Levy[14] L. Linssen[8] A. Ljubičić[23] J. Long[2,27] A. Lupi[7] E. Manola-Poggioli[1,8] A. Marchionni[7] F. Martelli[21] X. Méchain[18] J-P. Mendiburu[1] J-P. Meyer[18] M. Mezzetto[13] S.R. Mishra[3] L. Mossuz[1] G.F. Moorhead[11] P. Nédélec[1] Yu. Nefedov[6] C. Nguyen-Mau[9] D. Nordmann[5] D. Orestano[17] F. Pastore[17] L.S. Peak[19] E. Pennacchio[21] J-P. Perroud[9] H. Pessard[1] R. Petti[15] A. Placci[8] A. Pluquet[18] G. Polesello[15] D. Pollmann[5] B. Popov[6,14] C. Poulsen[11] P. Rathouit[18] G. Renzoni[16] C. Roda[16] A. Rubbia[8,24] F. Salvatore[15] K. Schahmaneche[14] B. Schmidt[5] M. Serrano[14] M.E. Sevior[11] D. Sillou[1] F.J.P. Soler[19] G. Sozzi[9] D. Steele[2,9] M. Steininger[9] U. Stiegler[8] M. Stipčević [23] T. Stolarczyk[18] M. Tareb-Reyes[9] G.N. Taylor[11] S. Tereshchenko[6] A. Toropin[12] A-M. Touchard[14] S.N. Tovey[11] M-T. Tran[9] E. Tsesmelis[8] J. Ulrichs[19] V. Uros[14] V. Vacavant[9] M. Valdata-Nappi[4,25] V. Valuev[6,1,10] F. Vannucci[14] K.E. Varvell[19,20] M. Veltri[21] V. Vercesi[15] D. Verkindt[1] J-M. Vieira[9] T. Vinogradova[10] M-K. Vo[18] S. Volkov[12] F. Weber[3] T. Weisse[5] M. Werlen[9] F. Wilson[8,28] L.J. Winton[11] B.D. Yabsley[19] H. Zaccone[18] K. Zuber[5] P. Zuccon[13]

[1]LAPP, Annecy, France
[2]Johns Hopkins Univ., Baltimore, MD, USA
[3]Harvard Univ., Cambridge, MA, USA
[4]Univ. of Calabria and INFN, Cosenza, Italy
[5]Dortmund Univ., Dortmund, Germany
[6]JINR, Dubna, Russia
[7]Univ. of Florence and INFN, Florence, Italy
[8]CERN, Geneva, Switzerland
[9]University of Lausanne, Lausanne, Switzerland
[10]UCLA, Los Angeles, CA, USA
[11]University of Melbourne, Melbourne, Australia
[12]Inst. Nucl. Research, INR Moscow, Russia
[13]Univ. of Padova and INFN, Padova, Italy
[14]14 LPNHE, Univ. of Paris, Paris VI and VII, France
[15]Univ. of Pavia and INFN, Pavia, Italy
[16]Univ. of Pisa and INFN, Pisa, Italy
[17]Roma-III Univ., Rome, Italy
[18]DAPNIA, CEA Saclay, France
[19]Univ. of Sydney, Sydney, Australia
[20]ANSTO Sydney, Menai, Australia
[21]Univ. of Urbino, Urbino, and INFN Florence, Italy
[22]IFIC, Valencia, Spain
[23]Rudjer Bošković Institute, Zagreb, Croatia
[24]ETH, Zurich, Switzerland
[25]Now at Perugia Univ., Perugia, Italy
[26]Now at UCSC, Santa Cruz, CA, USA
[27]Now at Univ. of Colorado, Boulder, CO, USA
[28]Now at Univ. of California, San Diego, USA

1 Introduction

We compare the fragmentation properties of the struck quark in Deep Inelastic Scattering (DIS) ν_μ N and $\bar{\nu}_\mu$ N charged current events to those of the quarks produced in e^+e^- annihilation and ep collider experiments. The comparison tests the universality of the quark fragmentation process in the region where non–perturbative effects become important. The neutrino data, accumulated in the NOMAD experiment [1], provide new precision measurements of the evolution of hadronic jets. The ν-data are complementary to the results from collider experiments: the space-time structure of the ν-interaction is different from those of the colliders and the region of the momentum transfer (Q) extends an order of magnitude below those accessible to the colliders.

The event kinematics of DIS are determined by the negative square of the four–momentum transfer, $Q^2 = -q^2$, and the Bjorken scaling variable, $x = Q^2/2P\cdot q$, where P is the four-momentum of the nucleon. In the Quark Parton Model (QPM), the interacting quark from the nucleon carries the four-momentum xP. The variable y, the fractional energy transfer to the nucleon in its rest frame, is related to x and Q^2 by $y = Q^2/xs$, where $\sqrt{s}$ is the lepton–nucleon centre of mass energy.

In the Breit frame [2] of DIS, the current region ($p_z < 0$) corresponds to the direction of the outgoing struck quark and the remnant region ($p_z > 0$) contains the nucleon remnant. In the QPM approximation the struck quark and nucleon remnant have momenta $-Q/2$ and $(1-x)Q/2x$ respectively. The properties of the ν_μ N current region at an energy of Q can be compared to e^+e^- annihilation measurements at an energy of $\sqrt{s}$.

Coherence effects in hadronisation are explicitly included in the Modified Leading Log Approximation (MLLA) [3] of perturbative Quantum Chromodynamics (pQCD). Long wavelength gluons are unable to resolve individual colour charges in the parton cascade, leading to a number of differences relative to the incoherent case. The two predictions investigated here are the slower rise in the mean multiplicity of charged partons, $\langle n_{ch}\rangle$, with increasing energy and the modification of the logarithmic scaled parton momentum spectra, $\ln(1/x_p)$, to an approximately Gaussian form known as the "hump-backed" plateau [4]. Here $x_p = 2p/Q$ and p is the momentum of a particle measured in the Breit frame.

Power corrections to hadronic event shape variables, such as thrust, or sphericity, are expected to have a characteristic $1/Q$ dependence. One approach to modeling these non–perturbative effects is based on an effective strong coupling constant which is approximately universal and differs from the perturbative form in the region below some energy cutoff μ_I [5,6]. The mean value of an event shape variable $\langle F\rangle$ at a scale μ_R can be written as the sum of a perturbative and a power–corrected part:

$$\langle F\rangle^{pert} = F_1\alpha_s(\mu_R) + \left(F_2 + \frac{\beta_0}{2\pi}\ln\frac{\mu_R}{Q}F_1\right)\alpha_s^2(\mu_R) \quad (1)$$

$$\langle F\rangle^{pow} = \frac{16}{3\pi}a_F\frac{\mu_I}{\mu_R}\left[\overline{\alpha}_0(\mu_I) - \alpha_s(\mu_R) - \frac{\beta_0}{2\pi}\left(\ln\frac{\mu_R}{\mu_I} + \frac{K}{\beta_0} + 1\right)\alpha_s^2(\mu_R)\right] \quad (2)$$

where $\beta_0 = 11 - 10/3$, $K = 67/6 - \pi^2/2 - 25/9$, $F_{1,2}$ and a_F are the perturbative and non-perturbative parameters, and α_s is the strong coupling constant at a given scale. The perturbative part, Equation 1, is the second order QCD prediction in the $\overline{\rm MS}$ scheme at the

scale $\mu_R = Q$. The power–corrected part contains a free non–perturbative parameter $\overline{\alpha}_0(\mu_I)$ that can be interpreted as an effective strong coupling constant below the infrared matching scale $\mu_I \sim$ 2–3 GeV.

In this analysis we use the thrust as the event shape variable to be investigated. The thrust is calculated with respect to the current hemisphere axis $\mathbf{n} = \{0,0,-1\}$ and is defined as:

$$1 - \mathrm{T_z} = 1 - \frac{\sum_i \mid \mathbf{p}_i \cdot \mathbf{n} \mid}{\sum_i \mid \mathbf{p}_i \mid} = 1 - \frac{\sum_i \mid \mathbf{p}_i^z \mid}{\sum_i \mid \mathbf{p}_i \mid} \tag{3}$$

The sum is taken over all charged and neutral hadrons in the current region.

2 Event Selection

The neutrino data were obtained with the NOMAD detector [1] at the CERN SPS wide–band neutrino beam produced by 450 GeV p-Be collisions. The relative beam composition of ν_μ:$\overline{\nu}_\mu$ was 1:0.06 with the corresponding average energies of 23.6 and 22.7 GeV. The detector consisted of a 2.7 ton active drift chamber target, a transition radiation detector, a preshower, and an electromagnetic calorimeter inside a dipole magnetic field of 0.4T. Outside the magnetic field was an iron-scintillator hadronic calorimeter followed by steel absorbers instrumented with drift chambers to measure muons. The low density, 0.1g/cm^3, of the neutrino target largely composed of carbon and the precise measurement of individual emergent particles enabled sensitive searches for neutrino oscillation [7]. These unique features of NOMAD also enabled detailed measurement of the hadronic jets resulting in the present study. The data presented here correspond to 8.6×10^{18} protons on the target.

The ν_μ N ($\bar{\nu}_\mu$ N) induced charged current events were selected by demanding a final state μ^- (μ^+) identified by the muon chambers with a momentum greater than 2.5 GeV matched to the primary vertex. The kinematic variables were reconstructed by summing over charged and neutral particles assigned to the primary vertex and demanding at least two primary charged tracks. The charged particles not identified as electrons or muons were assumed to be pions. A cut of $\mathrm{Q}^2 > 1$ GeV rejected most of the non-scaling, quasi–Elastic (QE) and resonance events. To reduce the background from neutral current interactions, where a π/K might decay to a muon, two cuts were imposed. The transverse momentum of the muon with respect to the hadron jet ($\mathrm{P}^T_{\mu H}$) was required to be greater than 0.9 GeV and the asymmetry between the transverse momenta of the muon and the hadron system was required to be less than 0.3. A total of 59K ν_μ and 1K $\bar{\nu}_\mu$ events survived the cuts. The neutral current and the non-scaling backgrounds were estimated to be less than 0.2% and 0.1% respectively of the sample.

The kinematic variables and the Breit frame boost were reconstructed using the energy and direction of the scattered muon and the direction of the hadronic jet [8]. The choice of the jet direction, as opposed to its energy, is less susceptible to systematic shifts caused by escaping neutrals. The four-momentum vectors of the charged particles in the hadronic jets were boosted to the Breit frame and assigned to the current region if $p_z < 0$.

3 Event Simulation and Data Correction

The LEPTO 6.1 program was used to simulate charge current DIS events with first order electroweak corrections [9]. The QCD cascades and fragmentation were simulated using the Lund string fragmentation model for the hadronisation phase as implemented in JETSET 7.3 [9]. These were subsequently passed through a GEANT [10] based full detector simulation.

The Monte Carlo simulation was used to correct the data for event selection cuts, event migration between x and Q^2 intervals, detector effects and reconstruction efficiencies, and track migration between current and remnant hemispheres. Bin–by–bin correction factors for the thrust and $\ln(1/x_{\rm p})$ distributions were calculated by forming the ratio of the Monte Carlo distributions at the generator level to the reconstructed level. The overall $\ln(1/x_{\rm p})$ correction factors were less than 20% and were independent of $\ln(1/x_{\rm p})$ around the peak position. The correction factors for the multiplicity distributions were in the range of 5% to 20%. For the thrust the resulting overall correction factors were less than 10%.

4 Results

The reconstructed $\ln(1/x_{\rm p})$ distributions for charged particles are shown in the Figure 1a, in the range $1 < Q^2 < 100$ GeV^2 for four regions in x in the current region. The distributions are independent of x. This is not the case for the remnant region, shown in Figure 1b, where the peak position moves to higher $\ln(1/x_{\rm p})$ as x increases. The momentum carried by the remnant decreases as x increases and so the phase space and the maximum scaled momentum decrease at a given p/Q. For $\langle x \rangle \sim 0.52$, $\ln(1/x_{\rm p}) > -0.6$ while for $\langle x \rangle \sim 0.11$ there is a weaker cutoff at $\ln(1/x_{\rm p}) > -2.5$.

To investigate the effect of coherence, the peak position of the $\ln(1/x_{\rm p})$ distribution in the current region, $\ln(1/x_{\rm p})_{\rm max}$, was evaluated by fitting a Gaussian over a range around the peak position. This fit was motivated by the MLLA prediction for the form of the spectrum which can be approximated by a Gaussian distribution around the peak position, although only at sufficiently high energies. A suitable restricted range for the fit was $0 \lesssim \ln(1/x_{\rm p}) \lesssim \ln(Q/2\Lambda)$ where Λ is an effective scale parameter. The results are shown in Table 1 for $\Lambda = 0.25$ GeV. The systematic errors included the contributions from refitting the data with the systematic variations listed in Section 5. These were combined in quadrature with an estimate of the uncertainty on the fit obtained by varying the fit range. The relative contribution to the systematic error from the fit variation was $\sim 60\%$.

Figure 2 shows the distribution of $\ln(1/x_{\rm p})_{\rm max}$ as a function of Q for the NOMAD and ZEUS data and of $\sqrt{s}$ for the e^+e^- data. Over the NOMAD range, the peak moves from $\sim$ 0.7 to 1.8, equivalent to the momentum spectrum maximum increasing from $\sim$ 280 to 600 MeV. The change in $\ln(1/x_{\rm p})_{\rm max}$ can be approximated phenomenologically by the straight line fit $\ln(1/x_{\rm p})_{\rm max} = a + b\ln(Q/1)$ shown in Figure 2. The values obtained from the fit to the NOMAD ν_μ data are $b = 0.65 \pm 0.03({\rm stat}) \pm 0.06({\rm sys})$ and $a = 0.54 \pm 0.03 \pm 0.09$. The systematic errors are calculated by re-fitting the $\ln(1/x_{\rm p})$ distributions obtained according to the variations listed in Section 5 and combining the deviations from the central value of the fit parameter, b or a, in quadrature. Also shown is the energy dependence when $b = 1$ ($a = 0.054 \pm 0.012$) which would be appropriate if the QCD cascade were of an incoherent nature [11]. The observed gradient is clearly inconsistent with $b = 1$ and confirms that coherence effects are occurring.

Q range (GeV)	Q mean (GeV)	(a) $\ln(1/x_{\rm p})_{\rm max}$	(b) $\langle {\rm n_{ch}} \rangle$	(c) $\langle 1 - {\rm T_z} \rangle$
1.0–1.3	1.14	$0.69 \pm 0.02 \pm 0.07$	$0.32 \pm 0.01 \pm 0.10$	$0.560 \pm 0.004 \pm 0.022$
1.3–1.5	1.41	$0.72 \pm 0.01 \pm 0.07$	$0.55 \pm 0.01 \pm 0.06$	$0.540 \pm 0.004 \pm 0.015$
1.5–1.8	1.67	$0.85 \pm 0.02 \pm 0.07$	$0.75 \pm 0.01 \pm 0.06$	$0.500 \pm 0.004 \pm 0.010$
1.8–2.1	1.94	$0.96 \pm 0.02 \pm 0.07$	$0.93 \pm 0.01 \pm 0.07$	$0.472 \pm 0.003 \pm 0.012$
2.1–2.3	2.21	$1.03 \pm 0.01 \pm 0.06$	$0.87 \pm 0.01 \pm 0.11$	$0.445 \pm 0.004 \pm 0.011$
2.3–2.7	2.53	$1.12 \pm 0.01 \pm 0.06$	$1.24 \pm 0.02 \pm 0.07$	$0.422 \pm 0.003 \pm 0.007$
2.7–3.1	2.88	$1.23 \pm 0.01 \pm 0.06$	$1.21 \pm 0.02 \pm 0.06$	$0.387 \pm 0.003 \pm 0.012$
3.1–3.6	3.32	$1.34 \pm 0.01 \pm 0.10$	$1.39 \pm 0.02 \pm 0.06$	$0.350 \pm 0.003 \pm 0.006$
3.6–4.4	3.97	$1.46 \pm 0.01 \pm 0.10$	$1.67 \pm 0.02 \pm 0.06$	$0.322 \pm 0.002 \pm 0.008$
4.4–6.1	5.10	$1.59 \pm 0.01 \pm 0.10$	$1.82 \pm 0.03 \pm 0.15$	$0.262 \pm 0.002 \pm 0.010$
6.1–10.0	7.25	$1.81 \pm 0.02 \pm 0.11$	$2.05 \pm 0.05 \pm 0.12$	$0.201 \pm 0.003 \pm 0.007$

Table 1: The measured values of the a) scaled momenta peak; b) mean charged multiplicity and c) mean thrust in the Breit frame current region as a function of Q for ν_μ N. The first error is statistical and the second systematic.

Although the lever arm of the NOMAD data is short, the results are compatible with DIS [12] and e^+e^- annihilation experiments [13, 14].

Over the measured range of Q, the mean charged multiplicity, $\langle {\rm n_{ch}} \rangle$, increases by a factor of six as shown in Table 1. In Figure 3, the mean multiplicity in the current region is compared with inclusive mean multiplicity measurements from e^+e^-, ep and $\overline{\nu}_\mu$ p experiments as a function of energy [12, 15]. The solid line is the extrapolation of a QCD–motivated fit to higher energy measurements of the form $\langle {\rm n_{ch}} \rangle = a + b\exp(c\sqrt{\ln(Q^2/Q_o^2)})$ with $a = 2.527$, $b = 0.094$, $c = 1.775$ and $Q_o = 1.0$ GeV; the dashed line represents the MLLA predicted form of the energy dependence $\langle {\rm n_{ch}} \rangle = a\alpha_s^b \exp(c/\sqrt{\alpha_s})(1 + O(\sqrt{\alpha_s}))$ with $a = 0.067$, $b = 0.49$, $c = 2.265$ and $O(\sqrt{\alpha_s}) = 0.43$ [16]. $O(\sqrt{\alpha_s})$ represents corrections of size $\sqrt{\alpha_s}$ to the energy dependence. The NOMAD ν_μ data fall below both predictions but lie between the purely leptonic e^+e^- and the semi-hadronic ep data. The NOMAD $\bar{\nu}_\mu$ data are $\sim 25\%$ lower again.

The mean thrust $\langle 1 - {\rm T_z} \rangle$ given in Table 1 becomes smaller as Q increases. The $1 - {\rm T_z}$ spectra become narrower and more peaked at lower values as Q increases. The energy dependence of the mean thrust is compared to DIS ep data [17] and e^+e^- data [14, 18] in Figure 4. The e^+e^- thrust values are calculated with respect to the thrust axis at an energy $E = \sqrt{s}$ and do not correspond exactly to the ν_μ N thrust. The dashed line is the $O(\alpha_s^2)$ perturbative prediction and it can be seen that hadronisation contributions become increasingly prevalent at low energy. The dotted line is the reported fit to the sum of Equations 1 and 2 for the H1 data extended to lower Q. The solid line represents the fit to the NOMAD and H1 data at a scale $\mu_R = Q$ with α_s and $\overline{\alpha}_0$ as free parameters. The perturbative coefficients $F_1 = 0.053$, $F_2 = 3.45$ and the non–perturbative coefficients $a_F = 1$, $\mu_I = 2$ GeV are taken from [6, 17]. The result of the fit gives $\overline{\alpha}_0 = 0.508 \pm 0.003 \pm 0.070$ and $\alpha_s(M_Z) = 0.113 \pm 0.001 \pm 0.005$ with a $\chi^2/{\rm ndf} = 24.7/16$. A fit to the NOMAD data only (dot–dash line) gives $\overline{\alpha}_0 = 0.502 \pm 0.005 \pm 0.070$ and $\alpha_s(M_Z) = 0.112 \pm 0.002 \pm 0.005$ with a $\chi^2/{\rm ndf} = 13.6/9$. The first error is statistical and the second is theoretical. The theoretical error comes from the accuracy of the QCD calculations

and the choice of different possible scales. Varying F_1 and F_2 by their reported errors introduces changes $\delta\alpha_s = 0.0003$ and $\delta\overline{\alpha}_0 = 0.004$. Varying μ_I by ± 0.5 GeV causes changes of $\delta\overline{\alpha}_0 = 0.002$ with power corrections changes proportional to μ_I. However, if $\mu_R = Q$, the assumption in the power corrections that $\Lambda \ll \mu_i \ll \mu_R$ is no longer true for all μ_R. A variation in the renormalisation scale of $0.8Q < \mu_R < 1.5Q$ leads to changes of $\delta\alpha_s = ^{+0.005}_{-0.004}$ and $\delta\overline{\alpha}_0 = 0.07$. The good agreement at low Q indicates that the event shape can be well described by power corrections $\propto 1/Q$.

Although the value of $\alpha_s(M_Z)$, determined from the Q-evolution of $\langle 1 - \mathrm{T_z} \rangle$, agrees well — and seemingly with comparable precision — with those of other experiments [19], we feel that the theoretical error might be larger than the analysis yields.

5 Systematic Errors

A number of systematic checks were performed in order to investigate the sensitivity of the measured results. The selection cuts in Section 2 were independently varied by one sigma. These included changes in: the primary vertex formation, the cuts on $\mathrm{P}^T_{\mu H}$ and transverse momentum asymmetry, the cut on the muon momentum, and the cuts on the fiducial volume. We quantified the systematic errors due to the discrepancies in the track reconstruction in data and Monte Carlo. The error due to the assumption that all final state particles were pions was checked by assigning the proton mass to one of the final state hadron jet particles such that it be in the momentum range $1 < p < 4$ GeV and in the polar angular range $0.2 < \theta < 0.6$ radians, and repeating the analysis. The effects of Fermi motion of the nucleons was simulated by randomly assigning a three momentum to the nucleus selected from an isotropic distribution with a maximum momentum of 0.215 GeV [20]. The possible reinteraction of hadronic jet particles within the target nucleus were investigated using the NUCRIN package [21]. The possible effect of different structure functions on the result was checked by reweighting the default GRV–HO [22] by the CCFR [23] parametrisation.

The maximum systematic change in $\ln(1/x_\mathrm{p})$ was at the 1.5%–2.0% level. The $\langle \mathrm{n_{ch}} \rangle$ was most affected by the changes in the primary vertex formation: it was reduced by 9% at low Q and 5% in the highest Q bin. All other systematic errors in $\langle \mathrm{n_{ch}} \rangle$ were typically below 5%. The systematic errors in the $\langle 1 - \mathrm{T_z} \rangle$ variable were at the 0.2%–2% level.

The systematic variations from the above checks were combined in quadrature to yield the quoted systematic errors in Table 1.

6 Conclusions

Charged particle distributions were measured in the current and remnant region of the Breit frame in DIS neutrino–nucleon interactions at low Q^2. The current region distributions $\ln(1/x_\mathrm{p})$ are independent of x and show a dependence on Q. The best description of the data is achieved assuming coherence effects where the production of soft particles and the growth of the mean multiplicity is suppressed relative to the incoherent case. In the remnant region, the predicted dependence on x is observed.

A comparison of these charged particle distributions with those from ep collider experiments has been performed. The growth in $\langle \mathrm{n_{ch}} \rangle$ with Q is similar to that found in in ep exper-

iments. The evolution of $\ln(1/x_{\rm p})_{\rm max}$ has been measured and is consistent with that observed in e^+e^- experiments. The fragmentation properties of the struck quark from the nucleon in DIS that have been studied here are compatible with those from quarks created in e^+e^- annihilation. The observed charged particle spectra are consistent with the universality of quark fragmentation.

The increase of the thrust with Q has been compared to predictions using perturbative QCD calculations together with a model for describing non–perturbative effects at an energy an order of magnitude lower than previous measurements. The power correction terms decrease with the expected $1/Q$ dependence and can be described by a universal parameter $\overline{\alpha}_0$ that is consistent with values found in e^+e^- and ep experiments.

Acknowledgments

We thank the management and staff of CERN and of all the participating institutions for their generous support to the experiment. We thank Dr. Andrei Kataev for fruitful discussions. We thank the following funding agencies for their support:

Australian Research Council (ARC) and Department of Industry, Science, and Resources (DISR), Australia; Institut National de Physique Nucléaire et de Physique des Particules (IN2P3), Commissariat à l'Energie Atomique (CEA), Ministère de l'Education Nationale, de l'Enseignement supérieur et de la Recherche, France; Bundesministerium für Bildung und Forschung (BMBF, contract 05 6DO52), Germany; Istituto Nazionale di Fisica Nucleare (INFN), Italy; Russian Foundation for Fundamental Research (grant 96-02-18562), Institute for Nuclear Research of the Russian Academy of Sciences, Russia; Fonds National Suisse de la Recherche Scientifique, Switzerland; Department of Energy, National Science Foundation (grant PHY-9526278), the Sloan and the Cottrell Foundations, USA.

References

[1] NOMAD Collab., J. Altegoer *et al.*, Nucl. Instrum. Methods A 404 (1998) 96.

[2] R.P. Feynman, "Photon-Hadron Interactions", Benjamin, N.Y. (1972)

[3] Yu. Dokshitzer et al., Rev. Mod. Phys. **60** (1988) 373

[4] Yu. Dokshitzer, V. Khoze, A. Mueller and S. Troyan, "Basics of Perturbative QCD", Editions Frontières, Gif-sur-Yvette, France (1991), ISBN 2–86332–101–3.

[5] Yu.L. Dokshitzer and B.R. Webber, Phys. Lett. **B352** (1995) 451;
Yu.L. Dokshitzer and B.R. Webber, Phys. Lett. **B404** (1997) 321

[6] M. Dasgupta and B.R. Webber, The Euro. Phys. J. **C1** (1998) 539.

[7] NOMAD Collab., J. Altegoer *et al.*, Phys. Lett. **B431** (1998) 219.

[8] S. Bentvelsen, J. Engelen, P. Kooijman, Proceedings of the 1991 Workshop on Physics at HERA, DESY Vol. 1 (1992) 23

[9] G. Ingelman, LEPTO 6.1, Proceedings of the 1991 Workshop on Physics at HERA, DESY Vol. 3 (1992) 1366; T. Sjöstrand, Comp. Phys. Comm. **39** (1986) 347; T. Sjöstrand and M. Bengtsson, JETSET, Comp. Phys. Comm. **43** (1987) 367.

[10] The NOMAD detector simulation is based on GEANT 3.21, CERN Program Library Long Writeup W5013.

[11] E.R. Boudinov, P.V. Chliapnikov and V.A. Uvarov, Phys. Lett. **B309** (1993) 210

[12] ZEUS Collab, M. Derrick et al, Z. Phys. **C67** (1995) 93

[13] OPAL Collab., M. Akrawy et al., Phys. Lett. **B247** (1990) 617

[14] TASSO Collab., M. Althoff et al., Z. Phys. **C22** (1984) 307

[15] E31A Collab., M. Derrick et al., Phys. Lett. **B91** (1980) 470;
TASSO Collab., W. Braunschweig et al., Z. Phys. **C45** (1989) 193;
PLUTO Collab., Ch. Berger et al., Phys. Lett. **B95** (1980) 313;
DELPHI Collab., P. Abreu et al., Phys. Lett. **B372** (1996) 172;
JADE Collab., W. Bartel et al., Z. Phys. **C20** (1983) 187;
MARK I Collab., J.L. Siegrist et al., Phys. Rev. **D26** (1982) 969

[16] DELPHI Collab., P. Abreu et al., Z. Phys. **C50** (1991) 185

[17] H1 Collab., C. Adloff et al., Phys. Lett. **B406** (1997) 256

[18] OPAL Collab., P. Ackerstaff et al., Z. Phys. **C75** (1997) 193

[19] Review of Particle Physics, The Euro. Phys. J. **C3** (1998) 81.

[20] M. Sandel et al, Phys. Rev. **C20** (1979) 744

[21] K. Hanssgen and J. Ranft, Computer Physics Communications **39** (1986) 53

[22] M. Glück, E. Reya and A. Vogt, Phys. Lett. **B306** (1993) 391

[23] W.C. Leung et al., Phys. Lett. **B317** (1993) 655;
P.Z. Quintas et al., Phys. Rev. Lett. **71** (1993) 1307;
W.G. Seligman et al., Phys. Rev. Lett. **79** (1997) 1213.

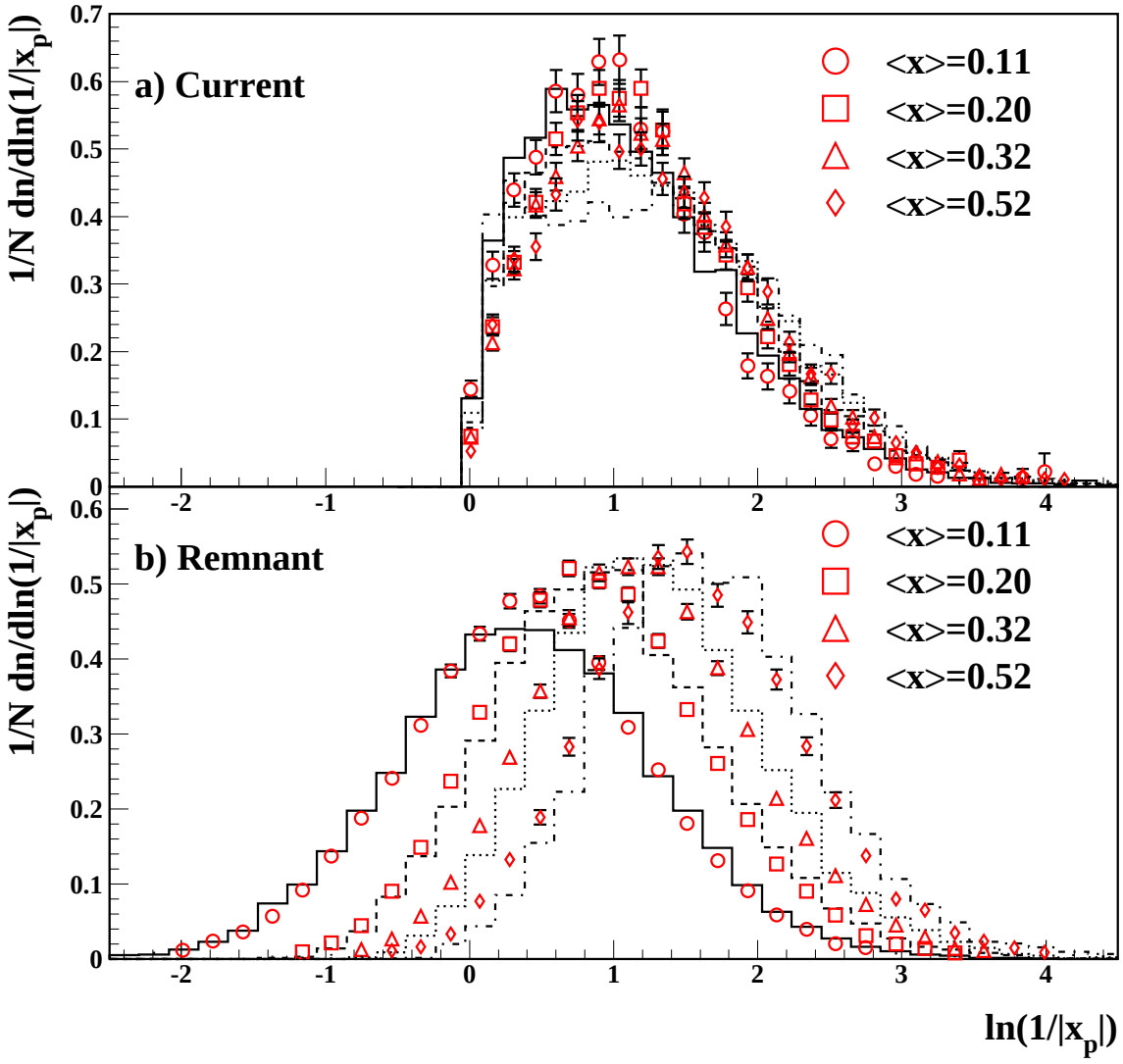

Figure 1: a) Reconstructed $\ln(1/x_{\rm p})$ distributions in the current region of the Breit frame as a function of x. b) Reconstructed $\ln(1/x_{\rm p})$ distributions in the remnant region. The histograms are the corresponding MC results. Only the statistical errors are shown.

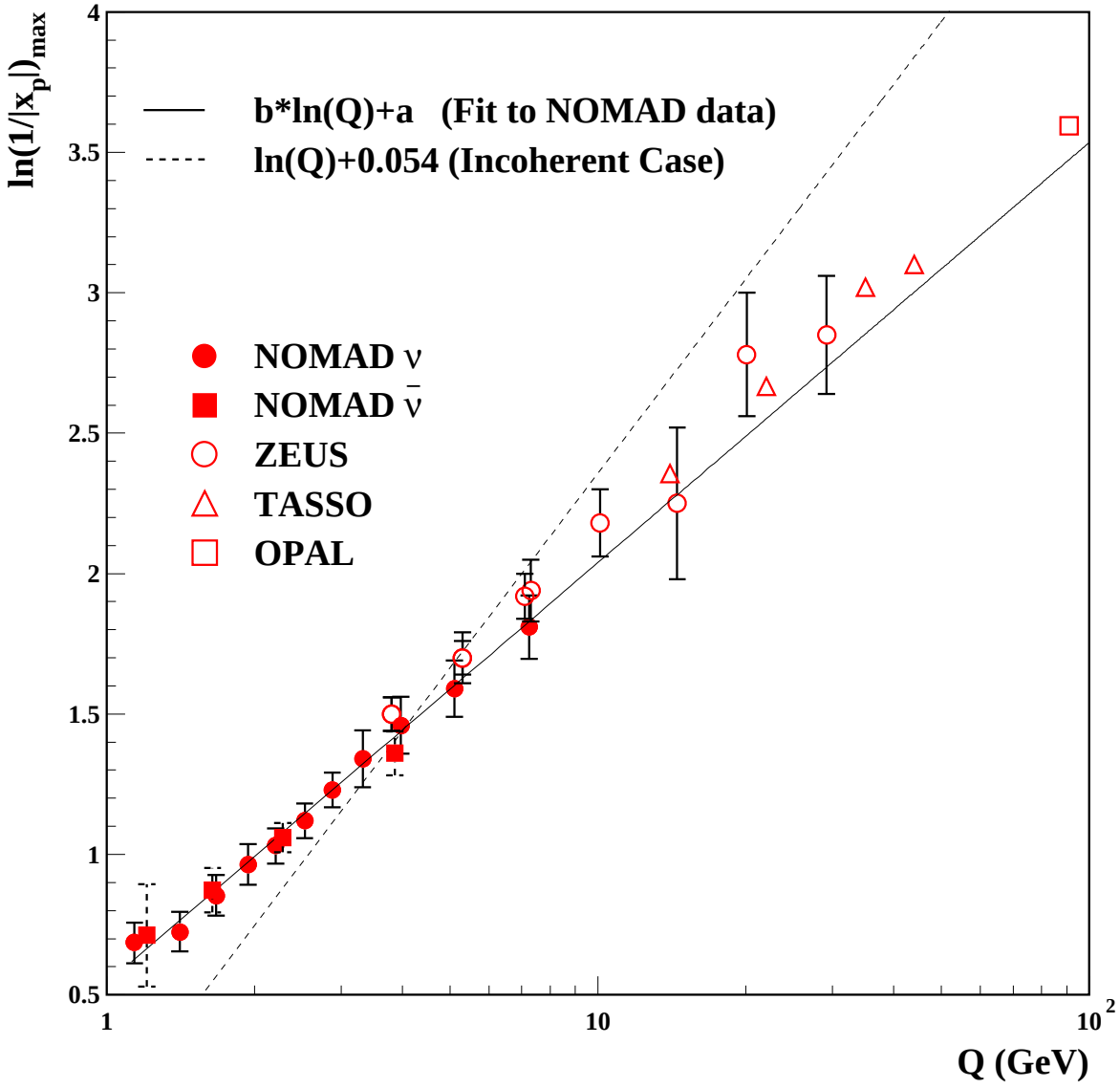

Figure 2: $\ln(1/x_{\rm p})_{\rm max}$ as a function of Q. The NOMAD data are compared to results from ZEUS, TASSO, and OPAL. A straight line fit of the form $\ln(1/x_{\rm p})_{\rm max} = b\ln(Q) + a$ to the ν_μ NOMAD $\ln(1/x_{\rm p})_{\rm max}$ values is indicated as well as the line corresponding to $b = 1$, discussed in the text. The NOMAD ν_μ points show the combined statistical and systematic errors from Table 1.

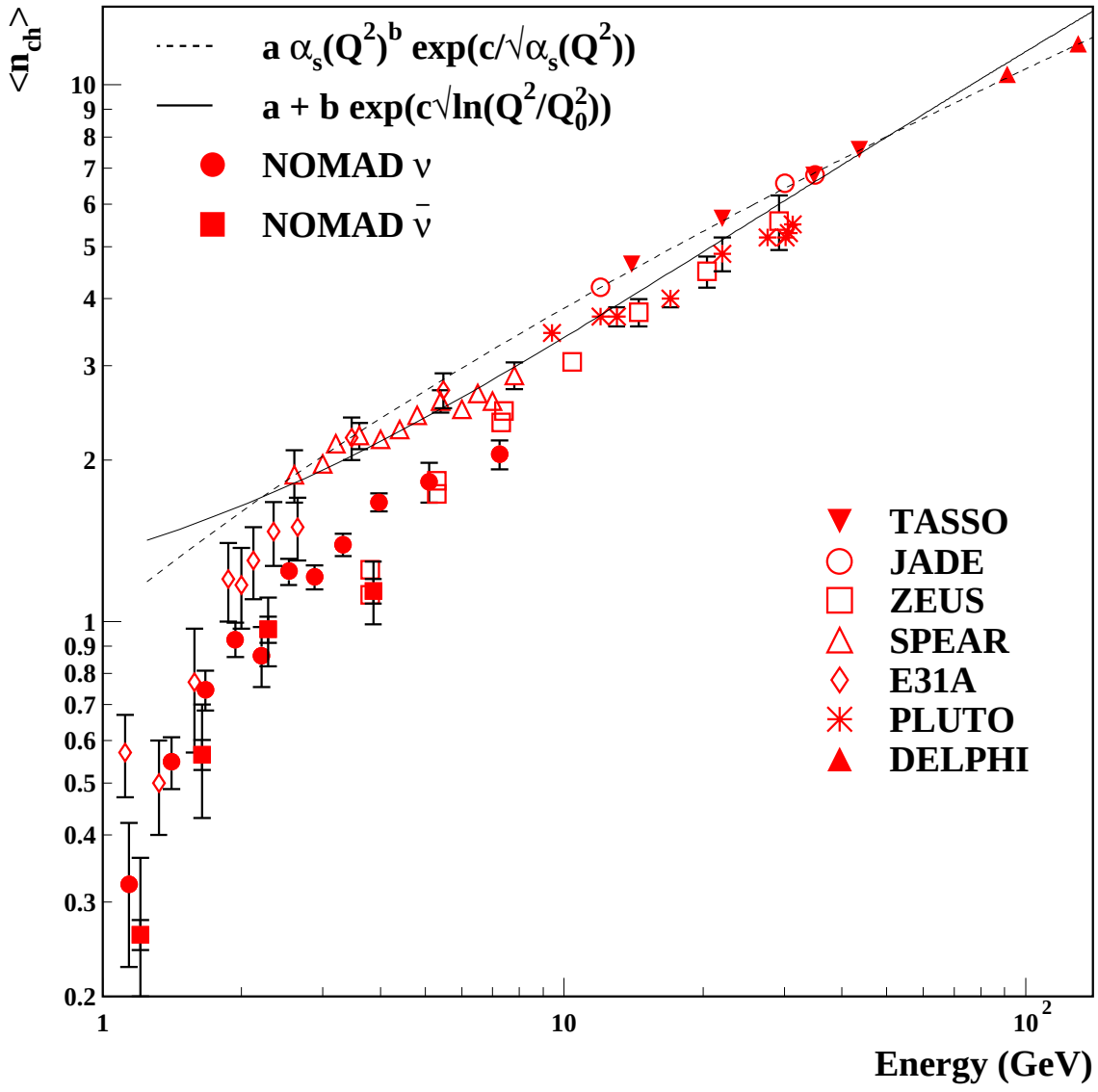

Figure 3: Mean charged multiplicity in the current region as a function of energy. The NOMAD multiplicity, $\langle n_{ch} \rangle$, is compared to $\langle n_{ch} \rangle/2$ results from e^+e^- experiments at energy $E = \sqrt{s}$ and $\langle n_{ch} \rangle$ from ep and $\overline{\nu}_\mu$ p experiments at $E = Q$. The NOMAD ν_μ points show the combined statistical and systematic errors from Table 1.

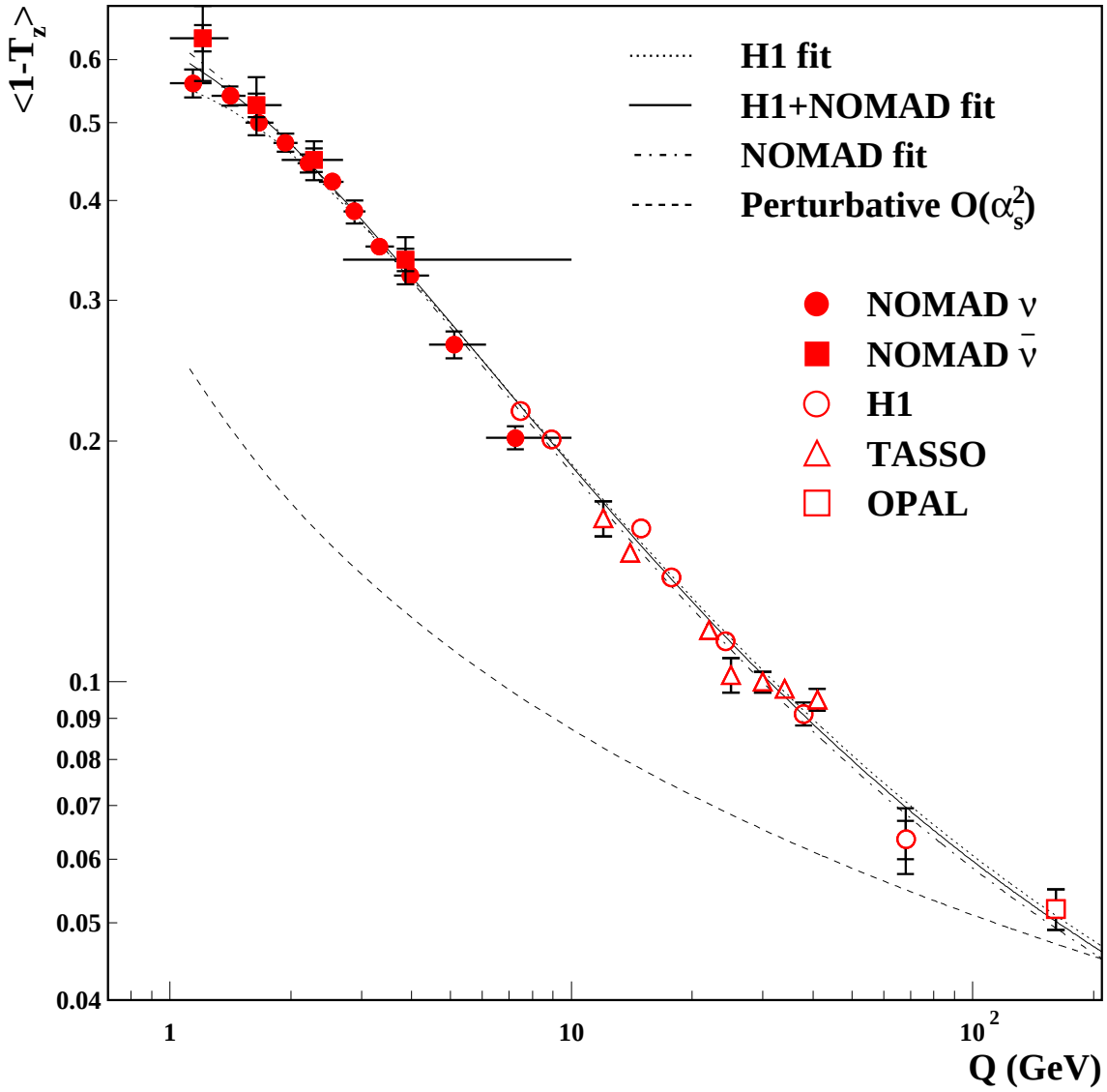

Figure 4: $\langle 1 - \mathrm{T_z} \rangle$ as a function of Q. The NOMAD data are compared to results from H1 and TASSO. The dotted line is the extrapolation of the MLLA fit to H1 data to NOMAD energies. The solid line is the fit including ν_μ NOMAD points. The dot–dash line is the fit to ν_μ NOMAD points only. The dashed line is the perturbative second order QCD calculation. The NOMAD ν_μ points show the combined statistical and systematic errors from Table 1.